J. Phys. Res. Edu., Vol. 2, March 2025

# High-energy heavy-ion collision and quark-gluon plasma

Provash Mali[1], Soumya Sarkar[2], and Amitabha Mukhopadhyay[1*]

[1] *Department of Physics, University of North Bengal, Darjeeling 734013, India*

[2]*Department of Physics, Siliguri College, Darjeeling 734001, India*

Some basic aspects of quark-gluon plasma and relativistic nuclear collisions are reviewed. General features of heavy-ion collisions like their space-time evolution, the thermodynamics and hydrodynamics of the intermediate fireball created therein, the phase diagram of QCD matter, the signatures of QGP formation etc., are summarily discussed. We expect that this introductory review will be able to draw a general interest among the graduate students to a very exciting area of physics.

## I. INTRODUCTION

The standard model of particle physics [1–3] explains the dynamics of all fundamental interactions of nature except gravitation. In particular quantum chromo-dynamics (QCD), a non-abelian gauge theory based on the color symmetry group $SU_c(3)$ [4], describes the interaction between quarks and gluons, the fundamental constituents of hadrons. Being a colored object the gluon is self-interacting. This leads to the *asymptotic freedom* [5, 6] and the *color confinement* [7]–two very important features of the strong interaction. At short distances (large momentum transfer $Q$), the quarks-gluons coupling becomes weak.

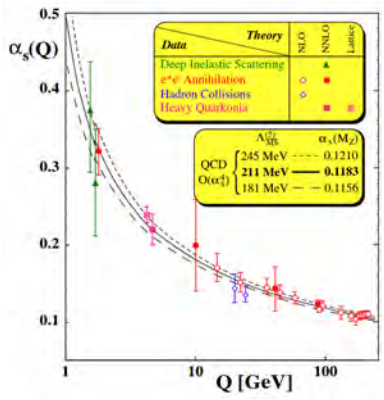


FIG. 1. Measured values of $\alpha_s(Q)$. Curves refer to the lQCD prediction [8].

The phenomenon indicates how quarks and gluons interact over a length scale of about 1 fm, and is perhaps

best described by the running coupling constant $(\alpha_s)$,

$$\alpha_s(Q) = \frac{12\pi}{(33 - 2n_f)\,\ln\left(\frac{Q^2}{\Lambda^2_{qcd}}\right)} \tag{1}$$

Here $\Lambda_{\rm qcd}$ ($\sim 200$ MeV) is a characteristic cut-off scale for the QCD, and $n_f$ represents the number of quark flavors in the theory. Figure 1 shows the variation of $\alpha_s$ with $Q$. Note that the experimental results nicely follow the lattice QCD (lQCD) prediction [8]. However, as $\alpha_s \to 1$, i.e. $Q^2 \sim \Lambda^2_{qcd}$, lattice calculation fails to work. In the $Q^2 \to 0$ limit, the quark-(anti)quark potential can be modeled by [9, 10],

$$V(r) = -\frac{4\,\alpha_s}{3r} + \kappa\, r, \tag{2}$$

The first term of Eq. (2) is similar to the Coulomb interaction, while the second term plays a key role in binding the quarks inside a hadron. At large distances $(r)$ the $q\bar{q}$-potential increases linearly with $r$. In fact the strong interaction is so strong, that if we try to pull apart a $q\bar{q}$-pair the strong force will resist the process very hard. As a result, if the potential energy exceeds the threshold of $q\bar{q}$ pair production, a new $q\bar{q}$-pair will be produced. Subsequently the process ends up producing two new color neutral hadrons. Isolated quarks have never been seen in nature.

QCD also predicts that quarks and gluons become weakly interacting at high temperature and pressure [11, 12]. The limiting temperature $(T_c)$ where hadronic matters turn into quark matter, according to the statistical bootstrap model [13], was found to be approximately 170 MeV. The hadronic density of states grows like,

$$\frac{d\rho}{dm} \sim m^{\alpha}\,\exp\left(\frac{m}{m_0}\right), \tag{3}$$

where $\alpha$ is a parameter and $m$ is the mass of the observed hadron having its rest mass $m_0$. The number of hadronic states within $E$ and $E + dE$ is [14],

$$dn(E) \sim dE \int_0^E p\,E\,\frac{d\rho}{dm}\,\exp\left(-\frac{E}{kT}\right) dm. \tag{4}$$

Under the limiting condition $E/m_0 \gg 1$ we get

$$dn(E) \sim E^{\alpha+3}\sqrt{\frac{\pi\, m_0^3}{2E^3}}\,\exp\left(\frac{E}{m_0} - \frac{E}{kT}\right) dE. \tag{5}$$

The total energy $E_{\rm tot} = \int E\, dn(E) \to \infty$ as $kT > m$. This is an indication that either beyond $m/k$ temperature cannot be defined, or there should be a new physics that describes the state.

The physics of color confinement-deconfinement transition has a significant implication in astrophysics and cosmology as well. It is assumed that [16, 17] at the very early stage of the universe all four fundamental forces of nature were unified into one fundamental interaction. Just after the big-bang, at a time scale of

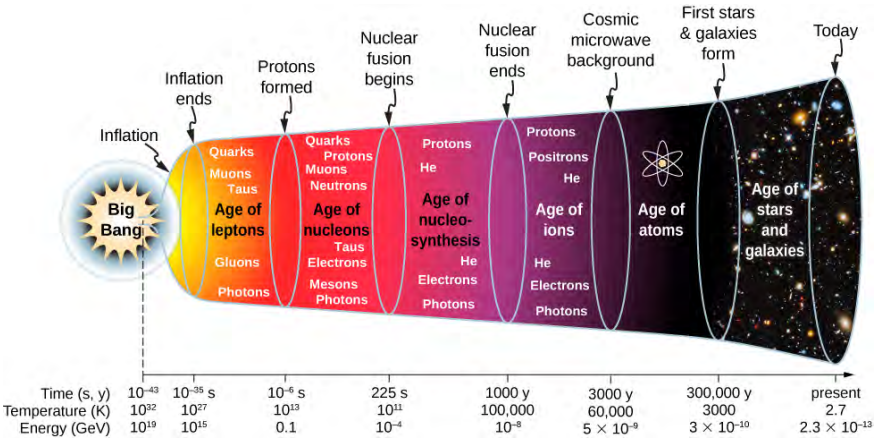


FIG. 2. A sketch presenting the timeline of the universe [15].

about $10^{-36}$s, the gravitational and strong interactions were separated. The universe expanded and cooled down rapidly, and went through a number of symmetry breaking processes. During the expansion fundamental particles like quarks and leptons were created. A plasma like state of quarks and gluons perhaps filled up the entire universe a few micro seconds after the big-bang [18]. Further cooling and expansion of the universe brought it to a state comprised of color neutral hadronic matter. The timeline from the big-bang to the present universe has been sketched in Figure. 2. According to some model calculations [19], a QGP like state is still expected at the core of compact astrophysical objects, such as the neutron stars. The inward strong gravitational pull for such objects creates color deconfinement. The temperature involved is much less than that of the big-bang, but the density of the matter $\rho \sim 10\rho_0$, where $\rho_0$ is the nuclear matter density. A typical heavy nucleus having $A \sim 200$ has a density $\rho_0 \approx 0.16$ nucleons/fm$^3$, and the corresponding energy density $\epsilon_N \approx 0.15$ GeV/fm$^3$. The QGP expected under this scenario will be rich in baryons. In a terrestial laboratory by colliding two heavy nuclei at high energies, QGP creation is possible either by vacuum heating (the big bang scenario), or by cold compression (core of compact stars).

## II. EXPERIMENTAL FACILITIES

The first generation of heavy-ion collision experiments began during the early 1970s in the Lawrence Berkeley National Laboratory (LBNL), Berkeley, and the Joint Institute for Nuclear Research (JINR), Dubna. The energy scale for the heavy ions was about a few GeV/nucleon, and for light ions it was $\sim 10$ GeV/nuclei. The results obtained from these experiments were mostly focused on multiparticle production and collective behavior of nuclear matter. The Alternating Gradient Synchrotron (AGS) at the Brookhaven National Laboratoty (BNL), USA, and the Super Proton Synchrotron (SPS) at the European Centre of Re-

search in Nuclear Physics (CERN), Geneva extended the energy scale by a few order of magnitude. The Schwer Ionen Synchrotron (SIS-18, and SIS-100) at the GSI, Darmstadt is another facility of heavy-ion collision research. The results produced from these experiments were not enough to confirm the creation of QGP, and required an energy enhancement. The Relativistic Heavy Ion Collider (RHIC) at the BNL was able to accelerate heavy-ions over the energy range $\sqrt{s_{\rm NN}} = 7.7$ to 200 GeV. Four major experimental facilities, namely the STAR, the PHENIX, the PHOBOS, and the BRAHMS were set up in the RHIC. The RHIC data provided an unambiguous signal of the QGP formation [20]. The Large Hadron Collider (LHC) at CERN further scaled up the energy upto $\sqrt{s_{\rm NN}} = 5.5$ TeV for the heavy-ions and $\sqrt{s_{\rm NN}} = 13$ TeV for the $pp$ collisions. Four major detector facilities, namely the ALICE, the ATLAS, the CMS, and the LHCb have been operating and collecting data from the year 2009. Contrary to the popular expectation, the QGP created in the LHC experiments, behaves more like an ideal fluid with a very low specific viscosity, rather than an ideal gas. In the recent past a few fixed target experiments like, the NA61/SHINE experiment at

| **Year** | **Accelerator** | **Projectile** | **Max. energy** |
|---|---|---|---|
| 1975 | Synchrophasotron, JINR | $^{12}$C, $^{24}$Mg, $^{20}$Ne, $^{28}$Si | $4.5A$ GeV |
| 1984 | Bevatron, LBNL | $^{12}$C, $^{40}$Ca, $^{84}$Kr, $^{238}$U | $2A$ GeV |
| 1986 | AGS, BNL | $^{28}$Si | $14.6A$ GeV |
| 1986 | SPS, CERN | $^{16}$O, $^{32}$S | $200A$ GeV |
| 1990 | SIS-18/100, GSI | $^{59}$Ni, $^{197}$Au | $2A$ GeV |
| 1992 | AGS, BNL | $^{197}$Au | $11A$ GeV |
| 1994 | SPS, CERN | $^{208}$Pb | $200A$ GeV |
| 2000 | RHIC, BNL | $^{197}$Au, $^{63}$Cu | $\sqrt{s_{\rm NN}} = 200$ GeV |
| 2008 | LHC, CERN | $^{208}$Pb, $^{131}$Xe | $\sqrt{s_{\rm NN}} = 5.5$ TeV |
| 2011 | SPS, CERN | $^{208}$Pb, $^{9}$Be, $^{40}$Ar, $^{131}$Xe | $158A$ GeV |
| 2015 | NICA, JINR | $^{20}$Ne, $^{24}$Mg | $\sqrt{s_{\rm NN}} = 3.7$ GeV |
| 2027 | SIS-300, GSI | $^{197}$Au, $^{208}$Pb, $^{238}$U | $40A$ GeV |

TABLE I. Chronology of commissioning the heavy-ion collision accelerator facilities.

the CERN-SPS, and the Compressed Baryonic Matter (CBM) experiment at the Facility for Anti-proton and Ion Research (FAIR), have been designed in order to explore the QGP state at high baryon density and low/moderate temperature. Beside the Nuclotron-based Ion Collider facility (NICA) at the JINR, Dubna is also capable of studying nuclear matter at high density. In Table I a chronology of the development of different accelerator facilities is summarily listed.

## III. NUCLEUS-NUCLEUS COLLISION AND QGP

A relativistic nucleus-nucleus $(AB)$ collision is a complex dynamical process. The energy and the size of the colliding nuclei are two controlling parameters of a collision. Heavy-ion collisions are preferred over $pp$ and hadronic collisions for the formation of a well equilibrated fireball medium, because a larger system leads to a rapid local thermal equilibrium. Apart from that an $AB$ collision allows multiple rescattering and higher multiplicities. Relative fluctuations in the particle number and measured thermodynamic quantities

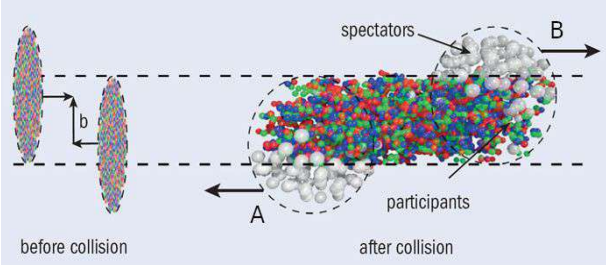


FIG. 3. Schematic of an $AB$ interaction.

are small in $AB$ collisions. If we consider an $AB$ collision as a superposition of a large number of nucleon-nucleon $(NN)$ collisions, then the equilibration time of the interaction would be $6 \times 10^{-34}$ sec. The hadron production time is taken to be $t = 0.2\, r_0\, A^{1/3}/c_s$, the time of contact for the colliding nuclei, where $c_s = \sqrt{1/3}\, c$ represents the speed of sound in an ideal gas of mesons. The factor $0.2$ is introduced since $50\%$ of the nuclear matter is contained within $0.2R$ of its surface depth. Figure 3 represents a high-energy $AB$ collision event. Due to their high speed the colliding nuclei will be Lorentz contracted in the longitudinal direction. Therefore, they appear like a pair of pancakes. The impact parameter $b \to 0$ implies a head on collision, while grazing or peripheral events have $b \to R_A + R_B$. An events sample comprised of all the allowed $b$ values is called the minimum bias sample. The nucleons that directly take part in the collision are called *participants*, and nucleons that do not participate are called *spectators*. The centrality of an $AB$ event can be measured in terms of (i) the number of participant nucleons $(N_{\rm part})$, (ii) the number of $NN$ binary collisions $(N_{\rm coll})$, (iii) the number density of produced particles, and (iv) the transverse energy deposited in the forward direction. Whereas the first two options can be used only for model calculations, in experiments the third and fourth parameters are commonly employed. The multiplicity of particles produced in an $AB$ interaction obviously depends globally on $\sqrt{s_{\rm NN}}$ and $b$, and locally on the transverse momentum $p_\perp$ and rapidity $y$. The low-$p_\perp$ region of the $p_\perp$-spectrum is called the thermal region and is described by an exponentially decaying function. This also represents collective nature of the medium present in the fireball system. On the other hand, the high-$p_\perp$ region of the spectrum provides information of hard scatterings, and it follows a power-law. The 'effective temperature' $(T_e)$ of the fireball is estimated from the slope of

 

the $p_\perp$-spectrum.

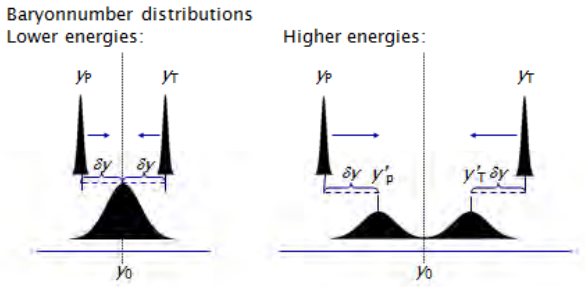


FIG. 4. A schematic of stopping in $AB$ collisions.

The central region of rapidity distribution in high-energy nuclear collisions is known as the central particle producing region, while the tails represent the fragmentation regions pertaining to the outgoing spectator fireballs. At ultra-high energies ($\sqrt{s_{\rm NN}} \sim 10^2$ GeV) the colliding nuclei become transparent with respect to each other. While passing through the interacting zone the nucleons leave a trail of energy in the form of stretched out energy flux. The flux lines subsequently fragment to produce new particles. The nucleons continue to move out of the central regions and produce a downshift in the rapidity distribution. In contrast, at low collision energy ($\sqrt{s_{\rm NN}} \lesssim 10$ GeV) the colliding nuclei can significantly stop each other, the $NN$ interaction time increases which leads to more nucleons populating the central interaction zone. As a result the rapidity distribution becomes maximum at the central particle producing region. The rapidity distributions at the two extreme conditions, i.e. when the colliding nuclei are fully transparent, and when there is a complete stopping, are schematically represented in Figure 4. The rapidity gap $\Delta y = y_{_P} - y_{_T}$ between the projectile and the target qualitatively measures the central region of particle production. For fixed target experiments $y_{_T} = 0$ and $\Delta y = y_{_P}$, and $\cosh \Delta y = E_{_P}/m_{_P}$. In collider experiments the center of mass system (CMS) is at rest in the laboratory, and the projectile/target rapidity is $\Delta y/2$. The rapidity gap follows a relation like $\Delta y \propto \ln \sqrt{s_{\rm NN}}$ [21].

## IV. SPACE-TIME EVOLUTION OF $AB$ COLLISION

A schematic of the space-time evolution of the fireball medium created in high energy nuclear collisions is shown in Figure 5. The longitudinal direction represents the beam direction and the transverse direction represents the proper time. In the CM frame the figure represents the following stages of evolution with and without taking a QGP state into account.

**The pre-equilibrium stage**: In the figure nucleus $A$ and nucleus $B$ collide with each other at $t = 0$ fm/c. Just after the collision the hot and dense matter created is non-uniformly distributed in space, which plays an important role to generate the collective motion in the final state. If sufficient energy is deposited in the overlapping region of the colliding nuclei, partonic degrees of freedom may be excited within the fireball. Otherwise, a hadron gas like state will be produced which is dominated by mesons and/or baryons. This stage lasts for about $\lesssim 1$ fm/c and is called the pre-equilibrium state. Very little information about this stage is available.

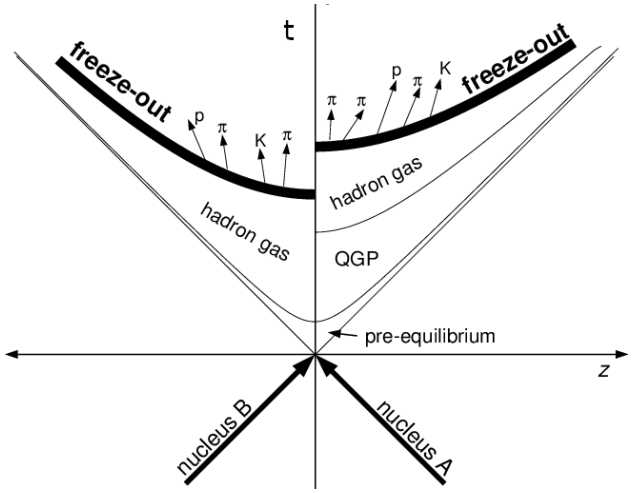


FIG. 5. A schematic of the space-time evolution of an $AB$ collision in the CM frame. The left hand side of the $t$-axis represents a hadron gas like situation without QGP, while the right hand side is with QGP.

**Thermalization**: Multiple (re)scattering among the constituent particles randomize the energy-momentum of the constituents particles, and brings the fireball medium to a thermally equilibriated stage. This stage may last as along as a few fm/c. If a QGP-like state is created, then the system will emit one or more QGP-observable and the system starts to expand radially and cools down.

**Hadron gas**: Hadronization is a process where partons recombine to form colorless bound state of hadrons. It might happen that for some time the intermediate fireball may remain in a mixed state of QGP and hadron gas (HG). If the energy density of the fireball is not sufficient to produce QGP, then the excitation energy of the interacting (participant) nucleons will be used to produce new particles, mostly low-mass mesons. At the last stage of hadronization the fireball system will be composed of newly produced hadrons which are weakly coupled, and forms an almost ideal gas of hadrons. If energy permits the newly produced hadrons will continue to exchange $q$ and $\bar{q}$ among themselves. This state is relatively short-lived, and hence it has

 

least influence on the evolution process of the fireball medium [22].

**Freeze-out**: As the fireball system expands further, the energy density drops down and inelastic interactions become irrelevant. The newly produced hadrons stop exchanging quarks among themselves, and hence the relative abundance of each hadron species becomes fixed. This is known as the *chemical freeze-out*. The elastic scattering among the particles may continue for another few fm/c after the chemical freezes out. During this period the newly produced particles achieve their final energy and transverse momentum, and finally come out of the interacting zone. This is referred to as the *kinetic freeze-out*. From the $p_{\perp}$-spectrum of the final state hadrons one can find out the freeze-out temperature and the radial flow velocity.

## V. THERMODYNAMICS OF THE FIREBALL

Some macroscopic properties of the intermediate fireball can be examined from the perspective of statistical mechanics, that can subsequently be used to explain some features of multiparticle production. The perturbation theory is not applicable in QCD due to the large value of $\alpha_s$, unless the colliding energy is extremely high. Under such a situation statistical calculation becomes an useful tool. It was none other than E. Fermi who first used statistical approach to study the high energy collision between two nuclei [23]. The theory is based on two assumptions: (a) the colliding nuclei release their energies within a sphere of volume $V = 2m_N V_0/\sqrt{s_{\rm NN}}$ and (b) the number of particles produced is large enough to create a thermodynamics state. Fermi proposed that an $n$-particle final state is related to the density of final states $\rho(E)$ as,

$$S(n) = \left[\frac{V}{(2\pi)^3}\right]^{(n-1)} \rho(E),$$

where the volume element $V_0 = 4\pi R_\pi^3/3$ is defined by the Lorentz contracted pion field range $R_\pi = 1/m_\pi$. Assuming that the pions are massless, the temperature of a system of $n$-hadrons is obtained as,

$$T^4 = \frac{3\,\varepsilon^2}{2\pi^2 V_0\, m_N} = \frac{9\varepsilon^2 m_\pi^3}{8\pi^3 m_N}.$$

These equations can be used to calculate the particle density and energy density in the final state.

### A. MIT bag model

The MIT bag model is a static idealization of the fireball created in nuclear collisions [24, 25]. In this model hadrons are considered as spherical enclosures (Bags) of radius $R$ that hold the quarks inside. The quarks and/or anti-quarks are massless inside the bag and infinitely massive outside. Quarks/anti-quarks

 

are spin-$\frac{1}{2}$ fermions, while the gluons are massless, spin-1 bosons. The system is treated as an ideal gas of massless relativistic particles. The quarks confined within the bag produce a degeneracy pressure which acts outwards. The energy-momentum conservation law is ensured by introducing the so-called bag pressure ($B$). The thermodynamics of the gas under different conditions is outlined below:

**Case (i) massless particles, $\mu = 0$:** Under this condition the number density of the $i$-th parton is given by,

$$n_i = \int \frac{d^3p_i}{(2\pi)^3} \frac{1}{\exp{(\beta\, E_i)} \pm 1}, \tag{6}$$

where the $+\,(-)$ sign refers to fermions (bosons), $E_i$ the single particle energy, and $\beta = T^{-1}$. Corresponding energy density is

$$\varepsilon_i = \int \frac{d^3p_i}{(2\pi)^3} \frac{E_i}{\exp{(\beta\, E_i)} \pm 1} \tag{7}$$

and the total energy is given by,

$$\varepsilon = \sum g_i\, \varepsilon_i = g^*\, \frac{\pi^2}{30}\, T^4. \tag{8}$$

In the above equation $g^* = (g_b + \frac{7}{8}\, g_f)$, where $g_b$ and $g_f$ are, respectively the degeneracy factors for bosons and fermions. This factor takes care of the charge, spin, flavor, color, etc. of the partons. For the three-flavor (baryons) and two-flavor (mesons) systems we get

$$\varepsilon_{qgp}(3\text{ flavor}) \;\approx\; 47.5\, \frac{\pi^2}{30}\, T^4 \quad \text{and} \quad \varepsilon_{qgp}(2\text{ flavor}) \;=\; 37\, \frac{\pi^2}{30}\, T^4. \tag{9}$$

Using the formulae for pressure $p = \varepsilon/3$ and entropy density $s = (\varepsilon + P)/T = 4\,\varepsilon/3\,T$, the entropy per particle is evaluated as,

$$\frac{s}{n}\Big|_{\text{bosons}} = \frac{2\,\pi^4}{45\,\zeta(3)} \approx 3.6 \quad \text{and} \quad \frac{s}{n}\Big|_{\text{fermions}} = \frac{7\,\pi^4}{135\,\zeta(3)} \approx 4.2. \tag{10}$$

For a QGP consisting of only $u$ and $d$ quarks

$$p_{qgp} = 37\, \frac{\pi^2}{90}\, T^4 - B. \tag{11}$$

For the maximum pressure we set $p_{qgp} = p_{\max}$, i.e.

$$p_{\max}(T_c) = p_{qgp}(T_c) \;\;\Rightarrow\;\; T_c = \left(\frac{90}{34\,\pi^2}\, B\right)^{1/4} \approx 0.72\, B^{1/4}. \tag{12}$$

For a normal hadronic matter $B^{1/4} \approx 200$ MeV/fm$^3$. Using this value of $B$ we get $T_c(\mu = 0) \approx 144$ MeV. The energy density ($\varepsilon$) and the pressure ($p$) as functions of temperature $T$, as obtained from lattice calculation, are shown in Fig. 6 [26]. The energy density plot indicates a rapid increase in the effective

 

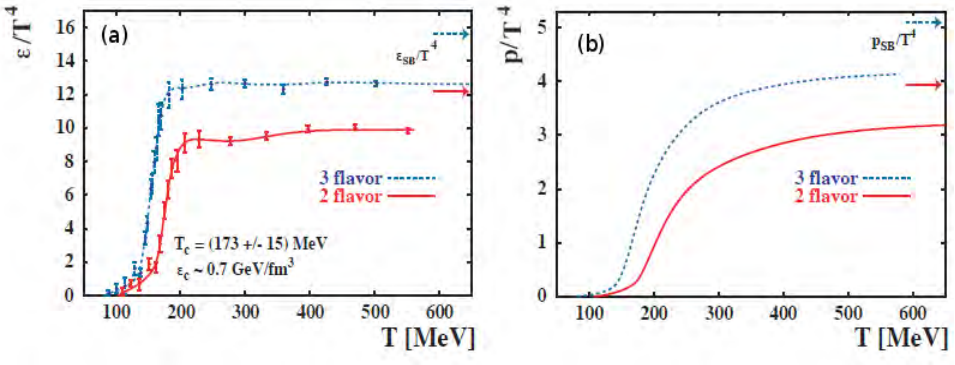


FIG. 6. (a) Energy density and (b) pressure of the QCD matter as functions of temperature [26]. The ideal Stefan-Boltzmann values are indicated by the (red) arrows.

degrees of freedom at $T_c \sim 170$ MeV. The chiral symmetry of the system is also restored at $T_c$. Plot (b) of the figure indicates that the pressure gradient $(dp/d\varepsilon)$ is reduced significantly during the hadron-QGP phase transition.

**Case (ii) massless particles, $\mu \neq 0$:** For non-vanishing $\mu$ the *grand potential* is given as,

$$\Omega(T,\, V,\, \mu) = -T\, \ln Z(T,\, V,\, \mu) = E\, -\, T\, S - \mu\, N = -p\, V, \tag{13}$$

and therefore the grand partition function

$$Z(T,\, V,\, \mu) = \text{Tr}\, \exp\left[\frac{\widehat{H} - \mu\, \widehat{N}}{T}\right] = \exp\left[-\frac{\Omega(T,\, V,\, \mu)}{T}\right]. \tag{14}$$

For low-mass bosons like pions, one can still consider the chemical potential to be zero. As the $q$ and $\overline{q}$ are produced in pairs, one can take $\mu_q = \mu_{\overline{q}}$. For a system of massless particles

$$\begin{aligned} T\, \ln Z|_{qgp} &= \frac{g_b V}{90}\, \pi^2\, T^4 + \frac{g_f V}{6\pi^2} \int p^3 \left[\frac{1}{\exp\{(E-\mu_q)/T\}+1} + \frac{1}{\exp\{(E+\mu_q)/T\}+1}\right] d^3p \\ &= V\left(\frac{37\,\pi^2}{90}\, T^4 + \mu_q^2\, T^2 + \frac{\mu_q^4}{2\,\pi^2}\right). \end{aligned} \tag{15}$$

The quark number density $(n_q)$ in the quark gas is given by,

$$n_{_q} = \left(\frac{T}{V}\right) \frac{\partial \ln Z|_{qgp}}{\partial \mu_{_q}} = 2\mu_{_q} \left(T^2 + \frac{\mu_q^2}{\pi^2}\right) \tag{16}$$

whereas the total number density of partons in a QGP system is,

$$n_{_{qgp}} = \frac{34\,\zeta(3)}{\pi^2}\, T^3 + 2\,\mu_{_q}^3. \tag{17}$$

For an ideal QGP system the energy density ($\varepsilon_{qgp}$) is given by, [27, 28],

$$\varepsilon_{qgp} = \varepsilon_q + \varepsilon_{\bar{q}} + \varepsilon_g = \left(\frac{T^2}{V}\right) \frac{\partial}{\partial T} \ln Z|_{qgp} + \mu_q\, n_q = \left(\frac{37\pi^2}{30}\, T^4 + 3\mu_q^2\, T^2 + \frac{3\mu_q^4}{2\pi^2}\right). \quad (18)$$

Corresponding pressure $P_{qgp}$ and the entropy density $s_{qgp}$ are,

$$P_{qgp} = \frac{T \ln Z|_{qgp}}{V} = \frac{37\,\pi^2}{90}\, T^4 + 3\,\mu_q^2\, T^2 + \frac{3\,\mu_q^4}{2\,\pi^2} \text{ and } s_{qgp} = \frac{\partial T \ln Z|_{qgp}}{\partial T} = \frac{74\,\pi^2}{45}\, T^3 + 2\,\mu_q\, T. \quad (19)$$

The entropy per particle is

$$\frac{s_{qgp}}{n_{qgp}} = \frac{74\,\pi^4}{45 \cdot 34\,\zeta(3)} \approx 3.92. \quad (20)$$

For a massless pion gas these numbers are,

$$\varepsilon_\pi = \frac{\pi^2}{10}\, T^4, \quad P_\pi = \frac{\pi^2}{30}\, T^4, \quad n_\pi = \frac{3\zeta(3)}{\pi^2}\, T^3, \quad s_\pi = \frac{2\pi^2}{15}\, T^3, \quad s_\pi/n_\pi \approx 3.6. \quad (21)$$

Though the QGP state possesses a higher degree of freedom than the hadron gas, the $s_\pi/n_\pi$-ratio is only about $9\%$ smaller than a typical QGP state. For a stable QGP state the Bag pressure is expected to be $P = \frac{1}{3}\varepsilon \geqslant B$. Accordingly, the limiting values of

$$\begin{aligned} &\text{the critical temperature } T_c\,(\mu_q = 0) = \left(\frac{90B}{37\pi^2}\right)^{\frac{1}{4}} \approx 147\,\text{MeV} \\ &\text{the chemical potential } \mu_c\,(T = 0) = \left(2\pi^2 B\right) = 0.43\ \text{GeV} \\ &\text{the baryon number density } n_c\,(T = 0) = \frac{2}{3\pi^2}\left(2\pi^2 B\right)^{\frac{3}{4}} = 0.72\ \text{fm}^{-3}. \end{aligned} \quad (22)$$

Taking the $qq$ and $q\bar{q}$ interactions into account, the energy density is expressed as [29],

$$\varepsilon = \left(\frac{37\pi^2}{30} - \frac{11\pi}{3}\alpha_s\right) T^4 + \left(1 - \frac{2}{\pi}\alpha_s\right) 3\mu_q^2 T^2 + \left(1 - \frac{2}{\pi}\alpha_s\right) \frac{3\mu_q^4}{2\pi^2}.$$

The Bag constant in terms of $T_c$ and $\alpha_s$ is then given by,

$$B = \left(\frac{37\pi^2}{90} - \frac{11\pi}{9}\alpha_s\right) T_c^4 + \left(1 - \frac{2}{\pi}\alpha_s\right) {\mu_c}^2 T_c^2 + \left(1 - \frac{2}{\pi}\alpha_s\right) \frac{{\mu_c}^4}{2\pi^2}.$$

Under the limiting conditions of $\mu_q = 0$ and $T = 0$

$$T_c(\mu_q = 0) = \left[\frac{B}{\left(\frac{37\pi^2}{90} - \frac{11\pi}{9}\alpha_s\right)}\right]^{\frac{1}{4}} \text{ and } \mu_c(T = 0) = \left[\frac{2\pi^2 B}{\left(1 - \frac{2}{\pi}\alpha_s\right)}\right]^{\frac{1}{4}}. \quad (23)$$

Both the critical temperature $T_c$ and the chemical potential $\mu_c$ depend upon $B$ and $\alpha_s$. The typical ranges of these parameters are $T_c \in (150 - 200)$ MeV and $\mu_c \in (450 - 600)$ MeV. Using a statistical model [30] it has been shown that the maximum net-baryon density is achieved at the SPS and FAIR energies. Such a result is shown in Figure 7, where the chemical freeze-out line is specified on the $(\rho_B,\, T)$-plane. The

 

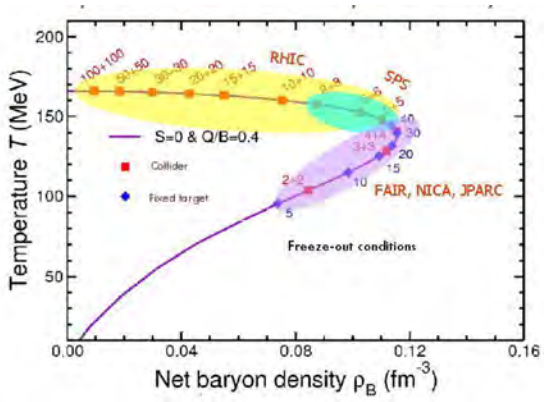


FIG. 7. Hadronic freeze-out line obtained from a statistical model [30].

beam energies from the FAIR to RHIC domain are shown by points on the diagram. It can be seen that the highest net-baryon density $\rho_B$ is created at beam energies in the range of $(25-40)$ GeV per nucleon. Calculations based on transport models estimate an energy density of about $2.5\ \mathrm{fm}^{-3}$ and a baryon density of about $(2-7)\rho_0$ at the center of the fireball, where $\rho_0$ is the baryon density of normal nuclear matter.

**Case (iii) – nucleon gas at $T = 0$:** This is a relevant situation for the study of compact astrophysical objects like neutron stars. For a degenerate Fermi gas of nucleons at $T = 0$ the partition function is expressed as,

$$T \ln Z|_N = \frac{g_N V}{6\pi^2} \int_0^\infty \frac{k^4\, dk}{E} \frac{1}{\exp[E-\mu]/T + 1}, \tag{24}$$

where $g_N 4 = 2$ (spin) $\times$ 2 (isospin) is the degeneracy factor. The nucleon number density $n_N$, the pressure $P_N$ and the energy density $\varepsilon_N$, are given by

$$\begin{aligned} n_N &= \frac{T}{V}\frac{\partial \ln Z|_N}{\partial \mu} = \frac{2M^3}{3\pi^2}\left(r^2-1\right)^{3/2} \\ P_N &= \frac{M^4}{6\pi^2}\left[r\sqrt{r^2-1}\left(r^2-\frac{5}{2}\right)+\frac{3}{2}\ln(r+\sqrt{r^2-1})\right] \\ \varepsilon_N &= \frac{T^2}{V}\frac{\partial \ln Z|_N}{\partial T} = \mu\, n_N - P_N = \frac{2\mu}{3\pi^2}\left(\mu^2-M^2\right)^{3/2} - P_N, \end{aligned} \tag{25}$$

where $r = \mu/M$, $M$ is the nucleon mass and $\mu$ is the nucleon chemical potential. The latent heat of QGP-hadron phase transition $L = \varepsilon_{QGP} - \varepsilon_N$ is given by,

$$L = \frac{2\mu_c}{3\pi^2} - \left[\left(\frac{\mu_c}{3}\right)^3 - \left(\mu_c^2 - M^2\right)^{3/2}\right] \tag{26}$$

The conservation of baryon number implies that $\mu_c = 3\mu_q = \mu/3$.

**Case (iv) – meson gas at $T \neq 0$:** The grand partition function as in this case is given as,

$$T \ln Z|_{m} \;=\; \frac{g_{M}\, V}{6\pi^2} \int_0^{\infty} \frac{k^4\, dk}{E} \frac{1}{\exp(E/T)-1} \;=\; \frac{g_{m}\, V\, T^2\, m^2}{2\pi^2} \sum_{n=1}^{\infty} K_2\left(\frac{nm}{T}\right). \tag{27}$$

Here, $m$ is the meson mass and $g_{M}$ is the mesonic degeneracy factor. $K_l$ is the modified Bessel function of degree $l$. The pressure of the gas is

$$P_{m} = \frac{T \ln Z|_{M}}{V} = \frac{g_{m}\, T^2\, m^2}{2\pi^2} \sum_{n=1}^{\infty} K_2\left(\frac{nm}{T}\right). \tag{28}$$

If we set $\mu_{m} = 0$, then the energy density $\varepsilon_{m}$ and the entropy density $s_{m}$ are given by

$$\varepsilon_{m} = 3\, P_{m} + \frac{g_{m}\, m^3\, T}{2\pi^2} \sum_{n=1}^{\infty} \frac{1}{n} K_1\left(\frac{nm}{T}\right) \quad \text{and} \quad s_{m} = 3\, \frac{P_{m}}{T} + \frac{g_{M}\, m^2}{2\pi^2} \sum_{n=1}^{\infty} \frac{1}{n} K_1\left(\frac{nm}{T}\right) \tag{29}$$

For baryons

$$\text{the pressure} \quad P_{B} = \frac{g_{B}\, m^2\, T^2}{2\pi^2} \sum_{n=1}^{\infty} \frac{(-1)^{n-1}}{n^2} K_2\left(\frac{nm}{T}\right) \times \left[\exp(n\mu/T) + \exp(-n\mu/T)\right],$$

$$\text{the number density} \quad n_{B} = \frac{g_{B}\, m^2\, T}{2\pi^2} \sum_{n=1}^{\infty} \frac{(-1)^{n-1}}{n} K_2\left(\frac{nm}{T}\right) \times \left[\exp(n\mu/T) - \exp(-n\mu/T)\right],$$

$$\text{the energy density} \quad \varepsilon_{B} = 3P_{B} + \frac{g_{B} m^3 T}{2\pi^2} \sum_{n=1}^{\infty} \frac{(-1)^{n-1}}{n} K_1\left(\frac{nm}{T}\right) \times \left[\exp(n\mu/T) + \exp(-n\mu/T)\right],$$

$$\text{the entropy density} \quad s_{B} = 3\frac{P_{B}}{T} + \frac{g_{B}\, m^3}{2\pi^2} \sum_{n=1}^{\infty} \frac{(-1)^{n-1}}{n} K_1\left(\frac{nm}{T}\right) \times \left[\exp(n\mu/T) + \exp(-n\mu/T)\right] \tag{30}$$

For a realistic scenario both the meson and baryon contributions are to be included into the hadron gas. Setting $\mu_{c} = 3\mu_{q} = \mu_{B}$ and $T = T_{c}$ at the phase boundary one gets $P_{QGP} = P_{B} + P_{M}$ and the latent heat $L = \varepsilon_{QGP} - (\varepsilon_{B} + \varepsilon_{M})$.

## VI. HYDRODYNAMICS OF THE FIREBALL

A simple picture of the space-time evolution of the central fireball medium can also be described by Hydrodynamics of heavy-ion collision. It assumes that the hot and dense fireball medium system is in local thermodynamic equilibrium. Without taking the details of any microscopic aspect into account, hydrodynamics allows us to describe the expansion of a fireball starting from the QGP, through hadronization and ending at the freeze-out. Hydrodynamics, although classical in concept and formulation, provides an important computational tool to describe the gross features of $AB$ collisions. It uses the energy-momentum conservation law to build an equation of state for the evolving medium. Here, we briefly describe two primary but different views of hydrodynamics, keeping in mind that the model has gone through significant modifications since its introduction.

 

**(i) Landau's model:** In an $AB$ collision the particles produced are mostly thermal pions having $p_{\perp} < 2$ GeV/c. These are called the 'soft' particles and are associated with the so-called soft processes. These particles give an overall idea of the collision dynamics. Landau's hydrodynamical model [31] gives us the extreme values of energy density, entropy, etc. of the fireball system when the colliding nuclei completely stop each other. It is assumed that the total available energy is transferred to produce new particles. For a symmetric nuclear collision Landau's model assumes that matter and energy accumulate at the mid-rapidity region of the fireball, and then the fireball experiences hydrodynamic expansion. The picture is similar to an ideal fluid in one-dimension. The maximum energy density obtained from the model is given by,

$$\varepsilon_{\max} = \frac{E_{cm}}{V_A} = \frac{3\,\gamma_{cm}\,\sqrt{s}\,N_{part}}{4\pi\,R^3} = \frac{3\,s\,N_{part}}{4\pi\,m_N\,R^3}. \tag{31}$$

Since a perfect fluid has no viscosity it can not produce entropy. Using simple thermodynamics of an ideal gas of massless particles we can write

$$s \propto \varepsilon^{3/4}, \qquad T \propto \varepsilon^{1/4}, \qquad \varepsilon \propto E_{cm}^2 \tag{32}$$

From the theory of black body radiation we get the number of produced particles $N \propto s$, and therefore, $N \propto E_{cm}^{1/2}$. The Lorentz contraction of the colliding nuclei produces large pressure gradient along the longitudinal direction. As a consequence the intermediate fireball predominantly evolves in the longitudinal direction. As it is assumed that the total energy of the colliding nuclei must be deposited, on an average the specific energy loss of the colliding nucleons must be greater than $\frac{E_{cm}/2}{(2R/\gamma_{cm})}$. The critical value of the specific energy loss is then defined as,

$$\left|\frac{dE}{dz}\right|_{cr} = \frac{E_{cm}/2}{(2R/\gamma_{cm})}. \tag{33}$$

At energies $\sqrt{s_{NN}} < 10$ GeV Landau's theory produces satisfactory results, while at the RHIC energies ($\sqrt{s_{NN}} \sim 10^2$ GeV) the model breaks down because of the small stopping power. Another downside of the theory is that the boundary conditions are defined at maximum density. The space-time correlation of particle production process is not embedded in Landau's theory, and hence the leading particle effect is ignored. As pointed out in [32, 33], these difficulties of Landau's model can be addressed properly if it is assumed that during the collision the valance quarks do not interact significantly, and the gluon fields are confined within the interaction zone. This requires that the gluon-gluon scattering cross-section has to be greater than the $qq$ scattering cross-section. In some recent works [34] the combination of Landau's relativistic hydrodynamics together with a constituent quark picture has been used to calculate the energy dependence of charged particle production in central nucleus-nucleus collisions. The model gives a fair

description of the experimental results over a wide range of $\sqrt{s_{NN}}$, from a few GeV to a few TeV.

**(ii) Bjorken's model:** Bjorjen's model of hydrodynamics is based upon two assumptions [35], (i) the medium produced after collision gets thermally equilibrated and then expands adiabatically and (ii) the central region of the rapidity distribution of the particles at the freeze-out is uniform. The dynamic of the medium is described by an equation of state (EoS) and a set of initial conditions, which are subjected to the conditions of local conservation laws [37, 38]. For an ideal non-dissipative fluid, the EoS can be derived from the relativistic tress energy tensor $T^{\mu\nu} = [\varepsilon + P]\ u^{\mu}\, u^{\nu} - P\, g^{\mu\nu}$, and charge-current density $j_B^{\mu} = [n_B(x)u^{\mu}(x)]$. Here the energy density $\varepsilon$, the pressure $P(x)$, the baryon number density $n_B$ and the four-velocity $u^{\mu} = (\gamma,\, \gamma\, \bar{v})$ are all defined at a point $x$ in the rest frame of the fluid. The equations of motion are derived from the tress energy tensor $T^{\mu\nu}$:

$$\partial_{\mu} T^{\mu\nu}(x) = \partial_{\mu}[\{\varepsilon(x) + P(x)\}u^{\mu}u^{\nu} - g^{\mu\nu}P(x)] = 0$$
$$\partial_{\mu} j_B^{\mu}(x) = \partial_{\mu}\left[n_B(x)u^{\mu}(x)\right] = 0. \tag{34}$$

In this theory all thermodynamic parameters depend only on $\tau = \sqrt{t^2 - z^2}$, the so called longitudinal proper time, and the longitudinal velocity $u_z = z/t = \tanh y$. The four-velocity $u^{\mu}$ = $(t/\tau, 0, 0, z/\tau)$ then reduces to

$$\frac{\partial \varepsilon}{\partial \tau} + \frac{\varepsilon + P}{\tau} = 0. \tag{35}$$

If we consider the following thermodynamic relation

$$\varepsilon + P = Ts + \mu_{_B} n_{_B} \tag{36}$$

and introduce the sound velocity $\lambda = dP/d\varepsilon$, then

$$\varepsilon(\tau_f) = \varepsilon(\tau_i)\left(\frac{\tau_i}{\tau_f}\right)^{1+\lambda}. \tag{37}$$

For vanishing net-baryon density

$$s(\tau_f) = s(\tau_i)\left(\frac{\tau_i}{\tau_f}\right) \quad \text{and} \quad T(\tau_f) = T(\tau_i)\left(\frac{\tau_i}{\tau_f}\right)^{\lambda}. \tag{38}$$

If the temperature exceeds the critical value for a QGP to hadron phase transition, the energy density and entropy of the medium increase rapidly, whereas the pressure rises slowly [Figure 6]. The EoS gets softer. At the end of the mixed phase the sound velocity $dP/d\varepsilon$ becomes minimum. The soft EoS also slows down the building-up of collectivity. In Bjorken's model the initial energy density is calculated assuming that all the particles are produced from a cylindrical volume which actually represents the overlapping region of the

 

colliding nuclei, and that the produced particles do not interact among themselves [35]. In the rest frame of the fluid let $A$ be the cross sectional area of the cylinder and its length be $v_z t$. The beam direction is taken along the $z$-axis and $z = 0$ is the point of interaction. Then a thin slab of thickness $dz = \tau \cosh y \, dy$ defines the overlapping volume element $\Delta V = A \, dz$. The energy density is given by [35],

$$\varepsilon_{BJ} = \frac{\Delta E}{\Delta V} = \frac{E}{A}\frac{dN}{dz} = \frac{m_t}{\pi R^2 \tau}\frac{dN}{dy} = \frac{1}{\pi R^2 \tau}\frac{dE_t}{dy}. \tag{39}$$

where $dN/dy$ is the rapidity density of the produced particles at $y = 0$ and the proper time $\tau \approx 1$ fm/c. For massless particles, $\varepsilon \propto T^4$ and $s \propto T^3$. Consequently, the final state energy density $\varepsilon_f = \varepsilon_i \, (\tau_i/\tau_f)^{4/3}$. This contradicts Bjorken's formula: $\varepsilon_{BJ} \sim \tau^{-1}$. Therefore, the energy density formula is modified as,

$$\varepsilon = \frac{1}{\pi R^2 \tau_0}\frac{dE_t}{dy}\left(\frac{\tau_f}{\tau_i}\right)^{1/3} = 2\,\varepsilon_{BJ}. \tag{40}$$

## VII. THE QCD PHASE DIAGRAM

The hadron-QGP phase transition can be represented on a baryon-density against temperature plot, popularly known as the QCD phase diagram. The phase diagram first introduced in the year 1975 [12], has evolved through a number of changes, as new phases find out their places in the diagram, and also new demarcation lines are drawn between different phases. A schematic of the diagram is depicted in Figure 8.

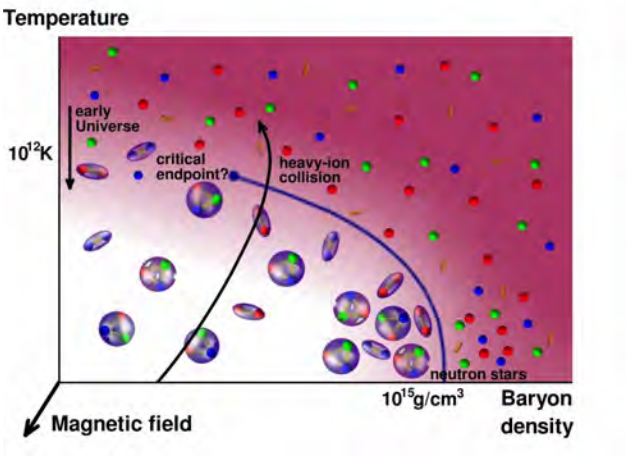


FIG. 8. A schematic representative of the QCD phase diagram [36].

The ordinary nuclear matter and hadron gas phases appear at lower values of temperature ($T$) and baryon density ($\rho$). To trigger deconfinement, that is to say, to probe the high-energy/density regime of QCD, an extreme environment is required. Two extreme realizations of interest are respectively, the high-$T$ and the high-$\rho$ region. The critical values of these parameters where the QGP to hadron gas (HG) transition is

expected to take place, are found to be $T_c \approx 150$ MeV ($\sim 10^{12}$K), and $\rho_c \approx 10^{15}$ g/cm$^3$ [39]. The baryon chemical potential $\mu_B$, a variable conjugate to $\rho$, may also be used along the horizontal axis. Theoretically, the values of the critical parameters and the nature of phase transition are sensitive to quark masses. If the up and down quarks are taken to be massless and other quark flavors to be infinitely heavy, then the QGP $\rightarrow$ HG phase transition will be of second order [40]. In contrast, if the up, down and strange quarks are considered as massless particles, then the transition seems to be first order [41]. Lattice calculation with realistic quark masses and for $\mu_B = 0$, predicts a smooth cross-over at low-$\mu_B$ and high-$T$ [42, 43]. The end point of the first order phase transition is known as a critical end point (CEP). The correlation length diverges at the CEP. Finding out the exact location of CEP is a topic of current research on heavy-ion physics. In order to pin point the location of CEP and to examine the QGP $\rightarrow$ HG phase boundary, fluctuations of conserved quantities and dynamical variables are measured at several different values of collision energy, which actually controls the temperature and density of the central fireball [44]. Besides the temperature and density, there are additional parameters such as the background magnetic field $B$, that might also be relevant to the QCD matter at extreme conditions. Studies on the magnetic field in hot and dense system is important from the perspective of early cosmology, because a certain class of neutron stars called magnetars, shows a very high degree of magnetic field [45]. In non-central heavy-ion collisions at the RHIC energies the induced magnetic field might be of the order of several $m_\pi^2$. Such a strong magnetic field competes with the strong interactions and introduces several new phenomena, for instance, it affects the chiral symmetry and its restoration, it induces a spatial asymmetry that results in a breaking of the Lorentz-symmetry, and also it modifies the hadron spectrum significantly. A recent review on the subject can be found in [46, 47].

## VIII. SIGNATURES OF QGP

The fireball medium created in a high-energy $AB$ collision, whether it contains a QGP state or not, can only be explored by some measurable parameters. Though, one has to rely on the produced particles that are recorded by the detector at a much later time, and trace back the sequence of events that have taken place in the intermediate stages of the collision. The particles originating from different stages of the collision process, should pass through the reaction zone and carry with them the information of the medium created. Some of these particles may be shadowed by a huge background noise, while some others may retain the QGP signal(s). Therefore, one has to be extremely careful while choosing an observable, so that it is almost insensitive to the process of hadronization. In this section we discuss several such QGP signals that are used to detect QGP formation in relativistic nucleus-nucleus collisions.

**Fluctuation of conserved charges:** Fluctuations of conserved quantities in high-energy nuclear collisions are widely studied to locate the position of the CEP on the QCD-phase diagram [48]. The $D$-measure of charge fluctuation is defined in terms of the total charge $N_{\rm ch}$ and the e-by-e variation of net charge $\delta Q$ as [49],

$$D = \langle N_{\rm ch}\rangle \left\langle \delta R^2 \right\rangle \approx 4\,\frac{\left\langle \delta Q^2 \right\rangle}{\langle N_{\rm ch}\rangle} \tag{41}$$

The variable is free from the volume effect of the primary and/or secondary sources of particle production. The variable $D$ has been measured using various models and under different experimental conditions, with and without taking the QGP-formation into account, and considering various final state effects [49–51]. For an uncorrelated pion gas $D \approx 4.0$ [51]. However, the $D$ measurement is influenced by various types of correlations and interactions, such as correlation arises from oppositely charged particle pairs, resonance decays, quark-quark interactions, etc. Taking all these effects into account, lattice QCD yields $D \approx 3.0$ for the HG, and $\approx 1.0 - 1.5$ for the QGP [51]. In the theoretical estimates of $D$-measure it has been assumed that the net-charge will vanish globally. In experiments however this is not always true. A more robust variable is defined as [52],

$$\nu_{\pm} = \left\langle \left( \frac{N_+}{\langle N_+\rangle} - \frac{N_-}{\langle N_-\rangle} \right)^2 \right\rangle \tag{42}$$

Here $N_+$ and $N_-$ are, respectively the number of positively and negatively charged particles in a collision event. The dynamical component of $\nu_{\pm}$, denoted by $\nu_{\rm dyn}$, will be nonzero when genuine particle corrections exist. The dynamical fluctuation does not depend on the detector efficiency. If all the charged particles emerging from an interaction are detected, the global charge conservation (GCC) will lead to a vanishing fluctuation. In such a case $\nu_{\pm,\rm dyn} = 4/\langle N_{\rm ch}\rangle_{4\pi}$, where $\langle N_{\rm ch}\rangle_{4\pi}$ is the multiplicity of charged particles for the $4\pi$ detector acceptance [52]. For an system of uncorrelated emission of particles $\langle N_{\rm ch}\rangle\,\nu_{\pm,\rm dyn}$ will be vanishingly small. If all the correlations are properly taken of, $\langle N_{\rm ch}\rangle\,\nu_{\pm,\rm dyn} \approx -1.0$ for a HG, and the product expected within $(-2.5, -3.0)$ for a QGP-like system.

**Collective flow:** Collective flow is considered as a dynamical response of the medium created in heavy-ion collisions. Anisotropy in the distribution of the participating nucleons, which is the main source of collective flow, directly influences the $p_{\perp}$-spectrum of the final state particles. In Figure 9 we show how an initial space anisotropy of a non-central $AB$ collision results in a final state momentum anisotropy, and consequently in the collective flow [53]. Collectivity reduces the azimuthal symmetric component of transverse or radial flow, and produces a steeper $p_{\perp}$-spectrum. Moreover, by boosting the radial flow, the shear viscosity renders the spectra flatter. It was estimated that in heavy-ion collisions, shear viscosity

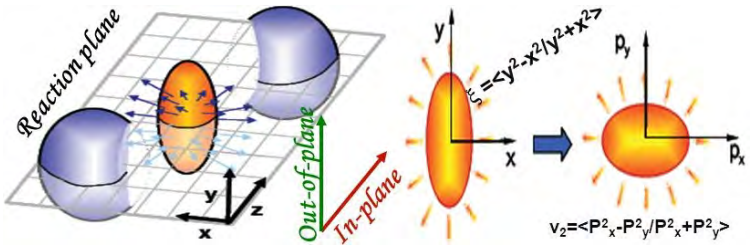


FIG. 9. A schematic representing how the initial anisotropy is originated in heavy-ion collisions which is manifested in collective phenomenon.

dominates over the bulk viscosity by a factor of about $5 - 10$ [54]. Although they are not easy to separate out in an experiment, because both of them modify the slopes of the $p_\perp$-spectra as well as the anisotropic flow. Hydrodynamic models with different EoS and initial conditions were used to quantify these effects [55].

The coefficients of anisotropic flow are measured from the following Fourier decomposition of the azimuthal distribution of the final state particles [56, 57],

$$\frac{d^3N}{d^3p} = \frac{1}{2\pi E\, p_\perp} \frac{d^2N}{dp_\perp\, dy} \left[1 + \sum_{i=1}^{N} 2\, v_n \cos\{n(\phi - \psi_{RP})\}\right], \tag{43}$$

where $\phi$ the azimuthal angle of the particle is measured with respect to the reaction plane, which is constituted by the beam (longitudinal) direction and the impact parameter of the collision. While the reaction plane angle $\psi_{RP}$ is the angle constituted by the reaction plane with the $x$-axis. The $n$-th harmonic of the above series is given as,

$$v_n = \langle\langle \cos n(\phi - \psi_{RP})\rangle\rangle, \tag{44}$$

where $\langle\langle \cdots \rangle\rangle$ indicates an averaging over all particles and all events within the kinematic region allowed by an experiment. The first harmonic $v_1$ measures the *directed flow*, $v_2$ measures the *elliptic flow*, and $v_3$ measures the *triangular flow*, and so on. The flow coefficients are sensitive to the initial density and geometry of the overlapping part, as well as to the the transport properties of the medium. Anisotropic flow measurements have demonstrated that the QGP produced at the LHC is one of the best examples of a nearly perfect fluid, so that the ratio of its shear viscosity to entropy density $\eta/s$ exhibits a minimum at the critical point of phase transition [58].

**Strangeness production:** The strange ($s$) quarks are not a priori present in fireball system created just after the collision. If energy permits strange particles are produced in high-energy $AB$ collisions [59, 60].

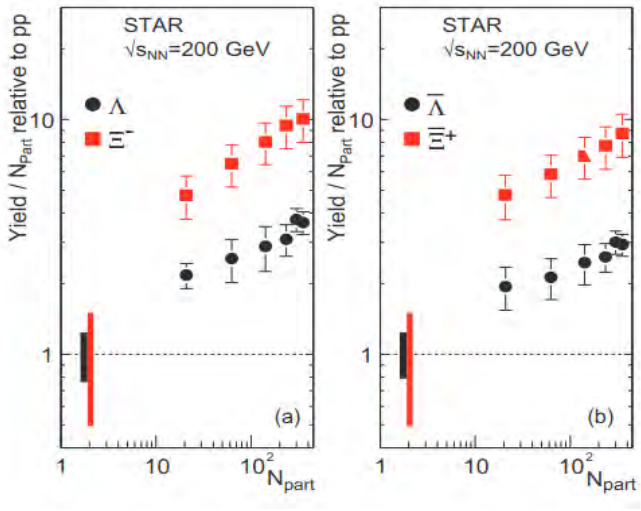


FIG. 10. Yield of strange particles $\Lambda$ and $\Xi$ in Au+Au collisions relative to $pp$ collision at $\sqrt{s_{NN}} = 200$ GeV [61].

The threshold energy for the strangeness excitation is considerably lower in QGP than in the hadronic matter [61]. Moreover, inelastic scattering of (thermal) gluons produces strange quark and enhances the strangeness content of QGP. Strangeness enhancement has been observed in the SPS [62], RHIC [63] and LHC [64] experiments. We illustrate the RHIC data in Figure 10, where the abundance of the strange particles $\Lambda$ and $\Xi$ are shown [61]. Note that the strange particles decay through weak interaction, which takes longer time than hadronization. Therefore, strange particles survive hadronization and carry forward undistorted information of the initial stages of the intermediate system.

**Charmonium production:** The charm particle, especially $J/\psi$, a bound state of $c$ and $\bar{c}$ quarks, are produced in hard $NN$ scattering. Color screening prevents the $J/\psi$ particles to sustain in a deconfined medium. The phenomenon is somewhat similar to Debye's screening in the electromagnetic plasma. Due to this reason a suppression in the $J/\psi$ yield in $AB$ collisions can be treated as a possible signature of QGP [66]. This is measured by the nuclear modification factor $R_{AA}$ defined as,

$$R_{AA}^{J/\psi} = \frac{1}{N_{ev}} \frac{d^2 N_{J/\psi}}{dp_T\, dy}\Big|_{\text{cent}} \Big/ \langle T_{AA} \rangle \frac{d^2 \sigma_{J/\psi}}{dp_T\, dy}\Big|_{pp}. \tag{45}$$

In the above equation $\sigma_{J/\psi}$ denotes the $J/\psi$ production cross-section in $pp$ collisions, $\langle T_{AA} \rangle$ is the nuclear overlap function in symmetric $AA$ collisions. Suppression of $J/\psi$ should result in $R_{AA} < 1$, and the signal has been measured at energies ranging from the SPS [67, 68] to LHC [69]. The results indicate that QGP is formed in nuclear collisions. Some recent results of the RHIC and LHC in this regard are shown in Figure 11. In contrast to the above, enhancement of charmonium states in relativistic $AB$ collisions has also been proposed as a possible signature of QGP formation. Since charm production is a hard process,

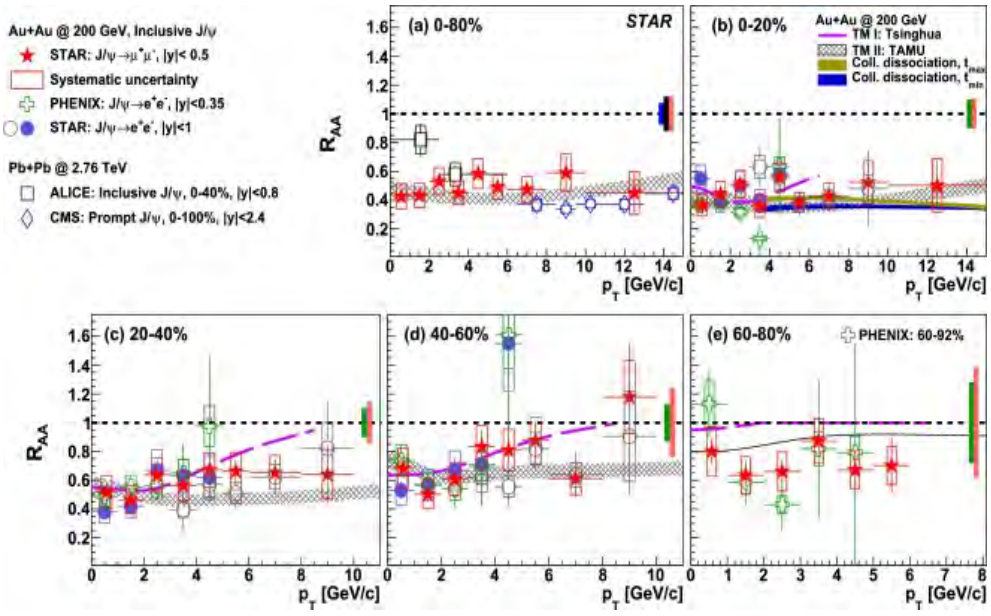


FIG. 11. $R_{AA}$ of $J/\psi$ with $p_T$ at different centralities. The RHIC and LHC results are compared with various model calculations [65].

it rapidly increases with increasing collision energy. At ultra-high energies and at its initial stages, the produced medium is expected to have more $c$-quarks as compared to a QGP medium. If the charm quarks recombine during hadronization and create charmonium states, an enhancement in the $J/\psi$ production will be observed, even if all primary (direct) $J/\psi$-s are dissociated [69].

**Jet quenching:** A bunch of relativistic particles moving in a direction is said to be forming a jet. In ultra-relativistic collisions fragmentation of partons, while passing through the reaction zone, results in jet production. To conserve momentum, jets are usually produced in pair, which is called di-jets. They move in opposite directions in the momentum space. When a di-jet is created near the surface of a partonic medium, one of the jets (away side jet) propagates through the partonic medium and the other one (near side jet) propagates through a hadronic medium. Under such circumstances the away side jet due to multiple rescattering that it goes through with the partons in the medium, will disappear or its energy will be reduced significantly. The phenomenon is known as *jet quenching* [70, 71], and it was first reported at the RHIC [72]. A schematic of jet-quenching is illustrated in Figure 12. The jet-quenching signal of QGP can also be measured in terms of the nuclear modification factor as defined in Eq. (45). Jet quenching is maximum in central collisions and it decreases monotonically from central to peripheral collisions, which confirms the formation of a deconfined partonic medium in central nuclear collisions. Recent progress on this topic is reviewed in [73, 74].

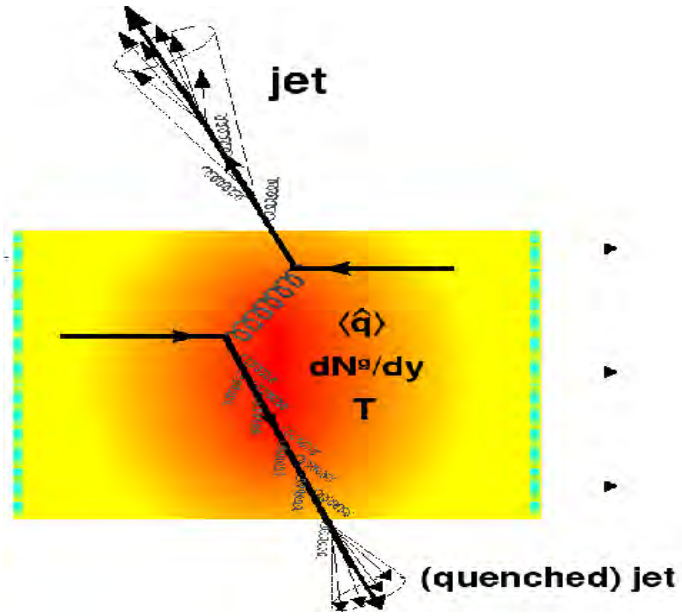


FIG. 12. Schematic of di-jet production.

## IX. CONCLUDING REMARKS

In this article we have reviewed some basic issues related to high-energy heavy-ion collision and quark-gluon plasma. Since it was first proposed that in order to create a QGP like state of weakly coupled partons, one should look into the intermediate stages of high-energy collisions between two heavy nuclei [75], the subject of high-energy heavy-ion collision has progressed significantly. It is now almost well established that a QGP-state, similar to what actually filled up the entire universe a few micro-seconds after its birth, has been created in heavy-ion experiments conducted at the RHIC and LHC. This particular research area has relevance in cosmology, astrophysics, QCD and high-energy physics. One good thing about high-energy heavy-ion physics is that, ever since the topic has been taken up as an area of research interest, both theory and experiment have almost always gone hand in hand. The topic requires expertise in several areas like the QCD, statistical mechanics, relativistic hydrodynamics, transport theory and computation. We believe that graduate students planning to pursue their research in this area, will find this introductory review quite useful.

* amphys@nbu.ac.in

[1] S. L. Glashow, Nucl. Phys. **22**, 579 (1961).

[2] A. Salam and J. C. Ward, Phys. Lett. **13**, 168 (1964).

[3] S. Weinberg, Phys. Rev. Lett. **19**, 1264 (1967).

[4] H. Fritzsch, M. Gell-Mann and H. Leutwyler, Phys. Lett. B **47**, 365 (1973).

[5] D. J. Gross and F. Wilczek, Phys. Rev. Lett. **30**, 1343 (1973).

[6] H. D. Politzer, Phys. Rev. Lett. **30**, 1346 (1973).

[7] K. G. Wilson, Phys. Rev. D **10**, 2445 (1974).

[8] S. Bethke, Nucl. Phys. Proc. Suppl. **121**, 74 (2003).

[9] J. Schwinger. Phys. Rev. **128**, 2425 (1962).

[10] A. Casher, J. Kogut and L. Susskind. Phys. Rev. D **10**, 1 732 (1974).

[11] J. C. Collins and M. J. Pery, Phys. Rev. Lett. **34**, 1353 (1975).

[12] N. Cabibbo and G. Parisi, Phys. Lett. B **59**, 67 (1975).

[13] R. Hagedorn, Suppl. Nuovo Cim. **3**, 147 (1965).

[14] W. Greiner, S. Schramm and E. Stein, *Quantum Chromodynamics*, 2nd ed. (Springer, 2002).

[15] https://www.civilsdaily.com/news/evolution-of-universe-after-the-big-bang

[16] E. W. Kolb and M. S. Turner, *The Early Universe* (Addison-Wesley, USA, 1990).

[17] J. Allday, *Quarks, Leptons, and the Big Bang* (Taylor and Francis, United Kingdom, 2002).

[18] E. V. Shuryak, Phys. Lett. B **78**, 150 (1978).

[19] G. Baym and T. Hatsuda *et al.*, Rep. Prog. Phys. **81**, 056902 (2018).

[20] P. Koch, B. Müller and J. Rafelski, Int. J. Mod. Phys. A **32**, 1730024 (2017).

[21] J. Letessier and J. Rafelski, *Hadrons and Quark-Gluon Plasma* (Cambridge University Press, Cambridge, UK, 2004).

[22] S. Afanasiev *et al.*, Phys. Rev. Lett. **99**, 052301 (2007).

[23] E. Fermi, Prog. Theo. Phys. **5**, 570 (1950).

[24] A. Chodos, B. L. Jaffe *et al.*, Phys. Rev. D **9**, 3471 (1974).

[25] A. Chodos, B. L. Jaffe, K. Johnson and C. B. Thorn, Phys. Rev. D **10**, 2599 (1974).

[26] F. Karsch and E. Laermann, *Quark-Gluon Plasma*, Eds. R. C. Hwa and X. N. Wang (World Scientific, Singapore, 2003).

[27] C. -Y. Wong, *Introduction to High-Energy Heavy-Ion Collisions* (World Scientific, 1994).

[28] R. Vogt, *Ultrarelativistic Heavy-Ion Collisions* (Elsevier, The Netherlands, 2007).

[29] D. Evans, QCD and the Quark-Gluon Plasma, Talk given in the Summaer School, Queen's University, Belfast, UK (2017).

[30] J. Randrup and J. Cleymans, Phys. Rev. C **74**, 047901 (2006).

[31] L. D. Landau, Izv. Akad. Nauk. Ser. Fiz. **17**, 51 (1953).

[32] P. Carruthers and M. Duong-Van, Phys. Rev. D. **28**, 130 (1983).

[33] L. Van Hove and S. Pokoroski, Nucl. Phys. B **86**, 243 (1975).

[34] E. K. G. Sarkisyan and A. S. Sakharov, Eur. Phys. J. C **70**, 533 (2010); *ibid.* **74**, 3147 (2014).

[35] J. D. Bjorken, Phys. Rev. D **27**, 140 (1983).

[36] Figure credit: http://www.sc.doe.gov/np/nsac/docs/Nuclear-Science.Low-Res.pdf

 

[37] K. Yagi, T. Hatsuda and Y. Miake, *Quark-Gluon Plasma, From Big Bang to Little Bang* (Cambridge University Press, Cambridge, 2005).

[38] P. Kolb and U. Heinz, *Quark-Gluon Plasma 3*, Eds. R. C. Hwa and X. N. Wang (World Scientific, 2003).

[39] A. Bazavov *et al.*, Phys. Rev. D **85**, 054503 (2012).

[40] R. D. Pisarski and F. Wilczek, Phys. Rev. D **29**, 338 (1984).

[41] M. A. Stephanov, Prog. Theor. Phys. Suppl., **153** 139 (2004).

[42] F. Karsch, E. Laermann and B. Peikert, Nucl. Phys. B **605**, 579 (2001).

[43] Z. Fodor and S. D. Katz, JHEP **03**, 014 (2002); JHEP **04**, 050 (2004).

[44] A. Korobitsyn, STAR Experiment Results from BES Program, Phys. Part. Nucl. **55**, 1037 (2024).

[45] R. C. Duncan and C. Thompson, Astrophys. J. **392**, L9 (1992)

[46] D. E. Kharzeev, K. Landsteiner, A. Schmitt and H. U. Yee, Lect. Notes Phys. 871 (2013).

[47] G. Bali, F. Bruckmann, M. Constantinou, M. Costa *et al.* PoS ConfinementX 198 (2012).

[48] V. Koch, M. Bleicher and S. Jeon, Nucl. Phys. A **698**, 261 (2002); *ibid* **702**, 291 (2002).

[49] S. Jeon and V. Koch, Phys. Rev. Lett. **85**, 2076 (2000).

[50] S. Gavin and C. Pruneau, Phys. Rev. C **61**, 044901 (2000).

[51] S. Jeon and V. Koch, Phys. Rev. Lett. **83**, 5435 (1999).

[52] C. Pruneau, S. Gavin and S. Voloshin, Phys. Rev. C **66**, 044904 (2002).

[53] H. Sorge, Phys. Lett. B **402**, 251 (1997).

[54] H. Song and U. Heinz, Phys. Rev. C **81**, 024905 (2010).

[55] J. Y. Ollitrault, Phys. Rev. D **46**, 229 (1992).

[56] S. A. Voloshin and Y. Zhang, Z. Phys. C **70**, 665 (1996).

[57] A. M. Poskanzer and S. A. Voloshin, Phys. Rev. C **58**, 1671 (1998).

[58] L. P. Csernai, J. I. Kapusta and L. D. McLerran, Phys. Rev. Lett. **97**, 152303 (2006).

[59] J. Rafelski and B. Müller, Phys. Rev. Lett. **48**, 1066 (1982).

[60] P. Koch, B. Müller and J. Rafelski, Phys. Rept. **142**, 162 (1986).

[61] J. Rafelski1 and J. Letessier, J. Phys. Conf. Series **50**, 176 (2006).

[62] F. Antonori *et al.* [NA57 Collaboration], J. Phys. G **32**, 427 (2006).

[63] B. I. Abelav *et al.* [STAR Collaboration], Phys. Rev. C **77**, 044908 (2008).

[64] K. Aamodt *et al.* [ALICE Collaboration], Phys. Lett. B **728**, 216 (2014).

[65] J. Adam *et al.* [STAR Collaboration], Phys. Lett. B **797**, 134917 (2019).

[66] T. Matsui and H. Satz, Phys. Lett. B **178**, 416 (1986).

[67] M. Gonin *et al.* [NA50 Collaboration], Nucl. Phys. A **610**, 404c (1996).

[68] M. C. Abreu *et al.* [NA50 Collaboration], Nucl. Phys. A **661**, 93 (1999).

[69] A. Adare *et al.* [PHENIX Collaboration], Phys. Rev. Lett. **98**, 232301 (2007).

[70] J. D. Bjorken, Fermilan-Pub-82-059-THY, Batavia (1982).

[71] G. -Y. Qin and X. -N. Wang, Int. J. Mod. Phys. E **24**, 1530014 (2015).

[72] J. Adams *et al.* [STAR Collaboration], Phys. Rev. Lett. **91**, 072304 (2003).

 

[73] M. Aaboud *et al.* [ATLAS Collaboration], Phys. Lett. B **790**, 108 (2019).

[74] S. Cao and X. N. Wang, Rep. Prog. Phys. **84**, 024301 (2021).

[75] T.D. Lee and G. C. Wick, Phys. Rev. D **9**, 2291 (1974).

 